# Geometric parametric instability in periodically modulated graded-index multimode fibers

C. Mas Arabí, A. Kudlinski, A. Mussot, and M. Conforti
*Univ. Lille, CNRS, UMR 8523-PhLAM Physique des Lasers Atomes et Molécules, F-59000 Lille, France*

(Received 16 November 2017; published 2 February 2018)

We present a theoretical and numerical study of light propagation in graded-index (GRIN) multimode fibers where the core diameter has been periodically modulated along the propagation direction. The additional degree of freedom represented by the modulation permits us to modify the intrinsic spatiotemporal dynamics which appears in multimode fibers. More precisely, we show that modulating the core diameter at a periodicity close to the self-imaging distance allows us to induce a moiré-like pattern, whereas a longer periodicity induces an adiabatic modulation or the self-imaging pattern. This complex dynamics modifies the geometric parametric instability gain observed in homogeneous GRIN fibers by generating new spectral peaks.

DOI: 10.1103/PhysRevA.97.023803

## I. INTRODUCTION

Parametric resonance (PR) is a well-known instability phenomenon which occurs in systems whose parameters vary in a periodic fashion. A classical example is a pendulum whose length changes harmonically with time. Depending on the system parameters, the pendulum may be unstable and the amplitude of its oscillations may become unbounded. Another example is the formation of standing waves on the surface of a liquid enclosed by a vibrating receptacle, a process known as Faraday instability [1]. Faraday instability manifests as pattern formation in several extended systems [2] and it has been studied in Bose-Einstein condensates (BECs) [3–6], granular systems [7], and chemical processes [8]. In these cases, the periodic modulation of the parameters is produced by an external forcing. However, the periodic variation may be self-induced by natural oscillations of the system as well. The emerging dynamics has been termed geometric parametric instability (GPI) [9] in the field of nonlinear optics or self-parametric instability in Bose-Einstein condensates [10]. Faraday instabilities and GPI can both be observed in fiber optics, which is a particularly interesting physical system for their study due to its simplicity. In nonlinear fiber optics, a continuous wave (cw) may be unstable, leading to the amplification of spectral sidebands. This effect is called modulation instability (MI) and is commonly associated with the anomalous dispersion regime [11], although it is also observed in the normal dispersion regime in the presence of higher-order dispersion [12], fiber birefringence [13], and multiple spatial modes [14,15]. A cw may also be unstable whatever the dispersion regime if a parameter of the system is varied periodically (an external periodic forcing is applied), leading to the observation of PR, which can coexist with standard MI in the same system [16–19]. This external forcing can result from periodic amplification [20], dispersion [21–25], or nonlinearity [26,27]. The periodic evolution of nonlinearity can be self-induced in highly multimode graded-index (GRIN) fibers. Indeed, such fibers exhibit a periodic self-imaging of the injected field pattern due to the interference between the different propagating modes [28]. This is due to the fact that the propagation constants of the modes are equally spaced and they have almost identical group velocity [29]. This creates a periodic evolution of the spatial size of the light pattern and therefore induces a periodic evolution of the effective nonlinearity in the propagation direction [30,31]. Recent experiments showed that PRs produced by this GPI can reach detunings from the pump on the order of hundreds of terahertzs [9].

In the present work we study GPI in a system having internal and external forcing with different periodicity. We consider a multimode GRIN fiber supporting self-imaging (at the origin of the internal forcing), with an additional modulation of the core diameter (inducing the external forcing). The overall longitudinal evolution of the spatial pattern exhibits two spatial frequencies. This results in the generation of characteristic spectral components which differ from the usual PR frequencies.

We consider two different regimes, which give rise to quite different GPI spectral components and have to be treated by different analytic tools. In the first case, the core modulation period and the self-imaging distance are close. The self-imaging intensity pattern along the fiber is thus modulated by a slow envelope, reminiscent of a moiré effect resulting from the beating of two similar frequencies. The resulting intensity profile can be calculated analytically by a multiple-scale expansion. In the second case, the core modulation period is much longer that the self-imaging distance. In this case the resulting intensity profile is again a slow modulation of the self-imaging pattern, but the longer period is now equal to the modulation period of the fiber core. In this case, multiple-scale expansion does not converge and Wentzel-Kramers-Brillouin approximation has to be used. The calculated patterns modulate the natural frequency of an equivalent oscillator, whose parametric resonances can be calculated by standard means and constitute the modified GPI spectrum, as we will show in the following.

The outline of the paper is as follows. After this introduction, in Sec. II we report numerical simulations illustrating the self-imaging pattern and the parametric instability spectrum for a modulated GRIN fiber. In Sec. III we calculate the cw evolution of the beam along the propagation coordinate, characterized by two spatial periods. In Sec. IV we study the

 

parametric instabilities generated by the spatial pattern when group-velocity dispersion is considered and provide estimates for the frequency of unstable bands. We summarize in Sec. V.

## II. PARAMETRIC INSTABILITY IN PERIODIC GRIN FIBERS

Spatiotemporal light propagation in multimode GRIN fibers can be described by the generalized nonlinear Schrödinger equation (GNLSE) [9,32]

$$i\partial_z E = \frac{1}{2\beta_0}\nabla_\perp^2 E - \frac{\beta_2}{2}\partial_t^2 E - \frac{\beta_0 g(z)}{2} r^2 E + \chi|E|^2 E, \quad (1)$$

where $E$ is the electric-field envelope measured in $\sqrt{\mathrm{W}}/\mathrm{m}$, $\nabla_\perp^2$ is the Laplacian over the transverse coordinates, $r^2 = x^2 + y^2$, $\beta_0 = k_0 n_0$ ($n_0$ being the refractive index at the core center and $k_0$ the vacuum wave number at the carrier frequency $\omega_0$), $\beta_2$ is the group-velocity dispersion, $g(z) = 2\Delta/\rho_c^2(z)$ [with $\rho_c(z)$ the fiber core radius and $\Delta$ the relative refractive index difference between core and cladding, $\Delta = (n_0^2 - n_{\mathrm{clad}}^2)/2n_0^2$], and $\chi = \omega_0 n_2/c$ is the nonlinear coefficient. We approximate the refractive index profile by $n^2(x,y,z) = n_0^2[1 - 2\Delta r^2/\rho_c(z)^2]$, so the waveguide is modeled as a pure harmonic potential with a depth varying along $z$. In the following, we restrict our study to light propagation over short distances (a few centimeters), so the linear coupling between modes due to fiber imperfections can be disregarded. Moreover, we assume that the fiber is excited with a Gaussian beam at the center so that the field presents circular symmetry. This allows us to solve Eq. (1) by means of a split-step Fourier method [11] in cylindrical coordinates [33], significantly reducing the numerical integration time.

It is worth noting that Eq. (1) shows some similarity to the Gross-Pitaevskii equation used in the field of Bose-Einstein condensates [3–6]. There are, however, two substantial differences: (i) BECs are usually studied in the repulsive case, which leads to a defocusing behavior, as opposed to the focusing Kerr nonlinearity of the fiber, and (ii) in BECs the dispersion operator has the same signs for all the transverse dimensions, whereas in fibers in the normal dispersion regime ($\beta_2 > 0$) that we will consider hereafter, dispersion and diffraction operators has different signs in Eq. (1).

We start by considering a uniform commercial GRIN fiber, whose parameters are reported in the caption of Fig. 1. By injecting into this fiber a Gaussian beam of size $a_0 = 20$ $\mu$m at a wavelength $\lambda_0 = 1064$ nm, a periodic light pattern is generated with a period $\xi = \pi/\sqrt{g_0} \approx 600$ $\mu$m ($g_0 = 2\Delta/\rho_0^2$). This can be observed in Fig. 1(a), which shows the evolution of the intensity in the core center $I(z) = |E(z,x=0,y=0)|^2$ (normalized to the input one) as a function of fiber length (normalized to the self-imaging period $\xi$). Figure 1(b) shows the output spectrum obtained at a normalized distance of 16, which exhibits three distinct GPI sidebands in the range 100–220 THz detuning from the pump. We then consider the propagation of the same input beam in a modulated fiber, with a period $L_{\mathrm{mod}}$ of 700 $\mu$m and a modulation depth of 3 $\mu$m. Figure 1(c) shows that the varying core diameter induces an additional modulation of the light intensity along the propagation. The self-imaging pattern is now modulated by an envelope of longer period $L$. As we will see hereafter,

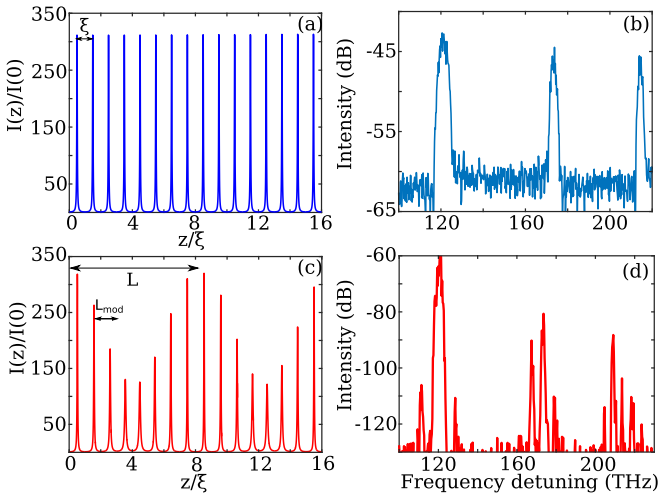


FIG. 1. Results obtained from direct numerical simulation of the GNLSE (1). (a) and (c) Evolution of the intensity in the core center normalized to the input one versus fiber length normalized to the self-imaging period $\xi$ in a fiber with (a) a uniform core and (c) a varying core. (b) and (d) Output spectrum in a fiber with (b) a uniform core and (d) a varying core. The parameters are typical of commercially available GRIN fibers: $n_0 = 1.47$, $n_2 = 3.2 \times 10^{-20}$ m$^2$/W, $\rho_0 = 26$ $\mu$m, $\Delta = 8.8 \times 10^{-3}$, $\lambda_0 = 1064$ nm, $a_0 = 20$ $\mu$m, fiber length (b) 1.4 cm and (d) 3 cm, $I_0 = 20$ GW/cm$^2$, and $\beta_2 = 16.55 \times 10^{-27}$ s$^2$/m.

$L$ depends on the relation between the natural self-imaging period $\xi$ and modulation period $L_{\mathrm{mod}}$. In the present example, $L_{\mathrm{mod}}$ is chosen to be close to $\xi$ and the resulting dynamics may be understood as a kind of moiré pattern. As shown in Fig. 1(d), this double periodicity in the spatial behavior produces new spectral bands around those obtained with a uniform fiber, in a similar fashion to what was observed in a single-mode dispersion-oscillating fiber with doubly periodic dispersion [34]. The process leading to the generation of these new spectral components will be analyzed and explained in the following sections.

## III. CALCULATION OF THE SELF-IMAGING PATTERN

To compute the spatial evolution of the beam profile, we start from Eq. (1), assuming cw propagation ($\partial_t = 0$):

$$i\partial_z E = \frac{1}{2\beta_0}\nabla_\perp^2 E - \frac{\beta_0 g(z)}{2} r^2 E + \chi|E|^2 E. \quad (2)$$

An approximated solution of Eq. (2) in the weakly nonlinear regime is a Gaussian beam with parameters varying along the propagation coordinate, which can be calculated by exploiting the method of moments [35] or variational techniques [36]. The solution reads

$$|E_s(x,y,z)|^2 = A_0^2\left(\frac{a_0}{a(z)}\right)^2 \exp\left(-\frac{r^2}{a(z)^2}\right), \quad (3)$$

where $a(z)$ is the solution of the following equation (overdots stand for the $z$ derivative):

$$\ddot{a} + g(z)a + \frac{C}{a^3} = 0, \quad C \equiv \left(\frac{n_2 a_0^2 A_0^2}{2n_0} - \frac{1}{\beta_0^2}\right). \quad (4)$$

The whole dynamics is thus ruled by the beam radius $a(z)$. Equation (4) is a singular nonlinear Hill equation of Ermakov type whose solution can be written as [37,38]

$$a(z) = \sqrt{u(z)^2 - \frac{C v(z)^2}{W^2}}, \tag{5}$$

where $u(z)$ and $v(z)$ are two linearly independent solutions of the equation

$$\ddot{x} + g(z)x = 0, \tag{6}$$

$W = u\dot{v} - \dot{u}v = \text{const}$ is the Wronskian, and the initial conditions are $u(0) = a_0, \dot{u}(0) = \dot{a}(0), v(0) = 0$, and $\dot{v}(0) \neq 0$. The linear Hill equation (6) is solvable in closed form only for very particular forms of $g(z)$ [39]. We consider here a harmonic modulation of the fiber core $\rho(z) = \rho_0[1 + \delta\cos(kz)]$, where $\delta$ describes the amplitude and $k = 2\pi/L_{\text{mod}}$ the period of modulation.

In the $(L_{\text{mod}}, \delta)$ plane, there are regions (known as Arnold tongues) where solutions of Eq. (6) become unbounded. This instability stems from the fact that the natural spatial frequency $k_{\text{nat}} \equiv \sqrt{g_0} = \sqrt{2\Delta}/\rho_0$ of the oscillator described by Eq. (6) is varied periodically with wave number $k$. The tips of the Arnold tongues fulfill the parametric resonance condition $k_{\text{nat}} = m(k/2)$ ($m$ integer), i.e., the natural spatial frequency is a multiple of half the wave number of the spatial forcing, which gives the following condition on the ratio between the modulation period and self-imaging distance:

$$L_{\text{mod}} = m\,\xi, \quad m = 1,2,\ldots. \tag{7}$$

When the condition (7) is not satisfied, the evolution of the beam size is periodic (or quasiperiodic) [39]. Moreover, even if the condition (7) is satisfied, there is a threshold on the modulation depth $\delta$ for the emergence of parametric instability, which in general increases for higher-order resonances. For the rest of the paper we assume to be in the absence of *spatial* parametric resonances.

Depending on the ratio between the modulation and self-imaging period, we can recover three different situations: $L_{\text{mod}} \ll \xi$, $L_{\text{mod}} \approx \xi$, and $L_{\text{mod}} \gg \xi$. The first case is the least interesting: In fact, the fast oscillating terms in Eq. (6) can be averaged out and the beam evolves as in a uniform fiber. The other two cases present quite peculiar behaviors, which are analyzed in detail below.

### A. Moiré pattern: $L_{\text{mod}} \approx \xi$

The most interesting case arises when $L_{\text{mod}} \approx \xi$ and the modulation depth $\delta$ is small enough to avoid unbounded evolution. By assuming a small modulation amplitude $\delta \ll 1$ and expanding $1/\rho(z)$ at second order in the small parameter $\delta$, Eq. (6) takes the following form:

$$\ddot{x} + \frac{2\Delta}{\rho_0^2}[1 - 2\delta\cos(kz) + 3\delta^2\cos^2(kz)]x = 0. \tag{8}$$

Two independent approximate solutions of Eq. (8) can be found by using multiscale techniques (see the Appendix):

$$u(z) = \frac{(4g_0 - k^2)a_0}{(4 + 2\delta)g_0 - k^2}\left[\cos(\sqrt{g_0}\sigma z) + \frac{\delta g_0}{k}\left(\frac{\cos[(\sqrt{g_0}\sigma - k)z]}{2\sqrt{g_0} - k} - \frac{\cos[(\sqrt{g_0}\sigma + k)z]}{2\sqrt{g_0} + k}\right)\right], \tag{9}$$

$$v(z) = -B\left[\sin(\sqrt{g_0}\sigma z) + \frac{\delta g_0}{k}\left(\frac{\sin[(\sqrt{g_0}\sigma - k)z]}{2\sqrt{g_0} - k} - \frac{\sin[(\sqrt{g_0}\sigma + k)z]}{2\sqrt{g_0} + k}\right)\right], \tag{10}$$

where

$$W = -B\frac{(4g_0 - k^2)a_0}{(4 + 2\delta)g_0 - k^2}\sqrt{g_0}\sigma, \tag{11}$$

$$\sigma = 1 + \frac{\delta^2(8g_0 - 3k^2)}{4(4g_0 - k^2)}, \tag{12}$$

and $B \neq 0$ is a constant, which does not appear in the expression of $a(z)$. Equations (9) and (10) give the expression of the beam radius through Eq. (5). A comparison between the beam evolution obtained from Eqs. (9) and (10) and the numerical solution of Eq. (4) is reported in Fig. 2, which shows remarkable agreement. In general, the solution is a combination of trigonometric functions of incommensurate arguments and thus is not strictly periodic. For small enough core radius modulation, we can safely assume $\sigma \approx 1$. In this case, the spatial behavior can be described as a combination of functions with period $\xi$ and functions with period $L_{\text{mod}}$. If we choose $L_{\text{mod}}$ and $\xi$ to be commensurate, the evolution of the beam is periodic with a longer period, which verifies $L = pL_{\text{mod}} = q\xi$ ($p$ and $q$ integers). In this regime, the resulting spatial behavior can be understood as a moiré pattern, where two patterns with close periodicity $\xi$ and $L_{\text{mod}}$ are superimposed, giving rise to a new longer periodicity $L$. If $L_{\text{mod}}$ and $\xi$ are incommensurate,

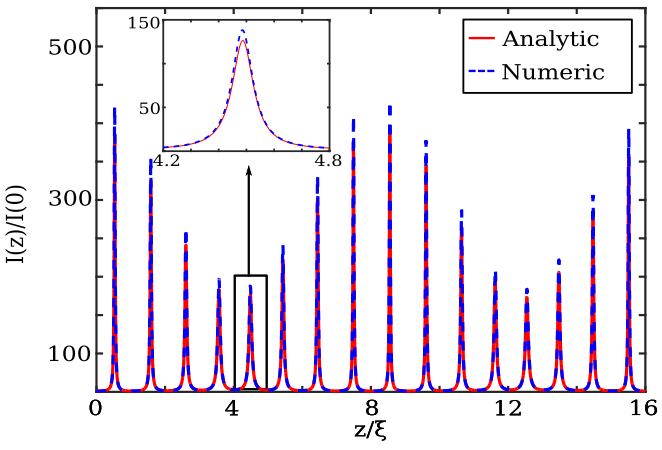


FIG. 2. Evolution of the intensity in the core center calculated from numerical solution of Eq. (2) (blue curve) and the exact solution (red curve) obtained from Eqs. (3), (5), (9), and (10). The parameters are the same as in Fig. 1(c).

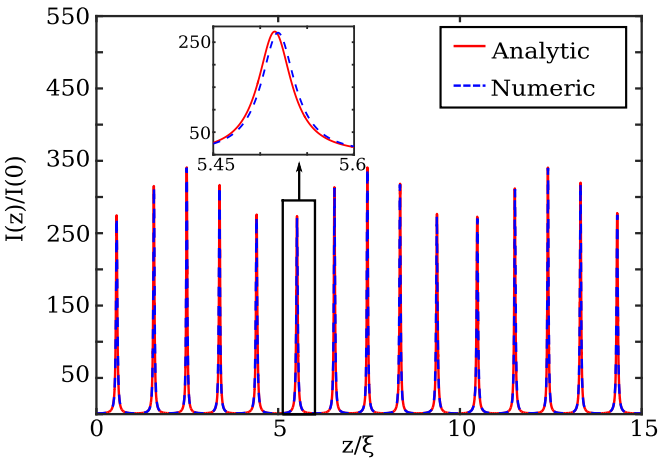


FIG. 3. Evolution of the intensity at the core center calculated from numerical solution of Eq. (4) (red dashed line) and the analytical solution (13) (blue solid line) for $L_{\rm mod} = 5\xi$. The other parameters are as in Fig. 1(c).

the evolution is only quasiperiodic. However, we can find the $p$ and $q$ that approximate the quasiperiodic evolution with periodic one with great accuracy. As we will illustrate below, the GPI spectrum resulting from a periodic or quasiperiodic evolution does not present qualitative differences.

### B. Adiabatic modulation: $L_{\rm mod} \gg \xi$

When $L_{\rm mod} \gg \xi$, variations over the intensity are adiabatic and we can use the Wentzel-Kramers-Brillouin approximation [40] to find two independent solutions $u(z)$ and $v(z)$ of Eq. (6), which inserted in Eq. (5) give the following expression for the beam size:

$$a(z) = \sqrt{a_0^2\sqrt{\frac{g(0)}{g(z)}}\cos^2[\phi(z)] - \frac{C}{a_0^2\sqrt{g(0)g(z)}}\sin^2[\phi(z)]}. \tag{13}$$

The phase $\phi(z) = \int_0^z dz'\sqrt{g(z')}$ reads

$$\phi(z) = \frac{2\sqrt{g_0}}{k\sqrt{1-\delta^2}}\left(\tan^{-1}\left[\sqrt{\frac{1-\delta}{1+\delta}}\tan\left(\frac{kz}{2}\right)\right] + \pi m\right),$$
$$m = \left\lfloor \frac{z}{L_{\rm mod}} + \frac{1}{2}\right\rfloor, \tag{14}$$

where $\lfloor x \rfloor = \max\{m \in \mathbb{Z} | m \leqslant x\}$. A comparison between the beam evolution obtained from Eqs. (13) and (14) and the numerical solution of Eq. (4) is reported in Fig. 3, which shows perfect agreement. We can see that the fast-varying self-imaging pattern of period $\xi$ is modulated adiabatically in a sinusoidal fashion by the longer period $L_{\rm mod}$ ($L_{\rm mod} = 5\xi$ in this example). When the amplitude of modulation tends to 0 ($\delta \to 0$), the phase simplifies to $\phi(z) \approx \pi/\xi z$. In this limit, the spatial behavior can be again described as a combination of functions with period $\xi$ and functions with period $L_{\rm mod}$. If $L_{\rm mod}$ and $\xi$ are chosen to be commensurate, the evolution of the beam is periodic with a longer period which verifies $L = pL_{\rm mod} = q\xi$, like the case where $L_{\rm mod} \approx \xi$. In the general case, where $\delta \neq 0$ we observe a self-imaging pattern modulated by an envelope of period $L = L_{\rm mod}$, which gives rise to a quasiperiodic behavior.

## IV. LINEAR STABILITY ANALYSIS AND GPI GAIN

We move now to the study of the stability of the cw spatial profile found in the preceding section with respect to time periodic perturbations. We assume a spatiotemporal field of the form

$$E(x,y,z,t) = [1 + \delta E(z,t)]E_s(x,y,z), \tag{15}$$

where $E_s$ is the approximated spatial electric field from Eq. (3) and $\delta E(z,t)$ is a small perturbation homogeneous in the transverse plane. By substituting the ansatz (15) in Eq. (1), after linearization we obtain

$$iE_s\partial_z\delta E = -\frac{\beta_2}{2}E_s\partial_t^2\delta E + \chi|E_s|^2E_s(\delta E + \delta E^*), \tag{16}$$

which projected on $E_s^*$ gives

$$i\partial_z\delta E = -\frac{\beta_2}{2}\partial_t^2\delta E + \frac{\chi A_0^2a_0^2}{2a(z)^2}(\delta E + \delta E^*). \tag{17}$$

A similar equation can be obtained when studying MI in single-mode fibers with oscillating nonlinearity [20–22,26]. By considering a time harmonic perturbation of the form $\delta E = a(z)e^{i\Omega t} + b^*(z)e^{-i\Omega t}$, we get the system

$$\begin{bmatrix}\dot a\\ \dot b\end{bmatrix} = i\begin{bmatrix}\frac{\beta_2\Omega^2}{2} + F(z) & F(z)\\ -F(z) & -\left(\frac{\beta_2\Omega^2}{2} + F(z)\right)\end{bmatrix}\begin{bmatrix}a\\ b\end{bmatrix}, \tag{18}$$

where

$$F(z) = \frac{\chi A_0^2a_0^2}{2a(z)^2}, \tag{19}$$

which can be reduced to a second-order ordinary differential equation for $y = a + b$:

$$\ddot y + \frac{\beta_2\Omega^2}{2}\left(\frac{\beta_2\Omega^2}{2} + 2F(z)\right)y = 0. \tag{20}$$

Since we have restricted our analysis to bounded evolutions of $a(z)$, the function $F(z)$ is (quasi)periodic as discussed in preceding section. In this case, Eq. (20) is again a Hill equation. Note that Eq. (20) rules the evolution of the time periodic perturbations, so an unbounded evolution for $y$ implies the instability of the cw field. The values of the perturbation frequency $\Omega$ for which the evolution of $y$ becomes unbounded gives thus the GPI spectrum.

### A. Constant core diameter

We start by considering a uniform fiber, which has already been studied in [32]. In this case the beam radius $a(z)$ assumes the simple expression

$$a^2(z) = a_0^2[\cos^2(\sqrt{g_0}z) + \mathcal{C}\sin^2(\sqrt{g_0}z)], \tag{21}$$

where $\mathcal{C} = (1-\mathcal{P})/\beta_0^2a_0^4g_0 = -C/g_0a_0^4$ and $\mathcal{P} = n_2\beta_0^2A_0^2a_0^2/2n_0$ is a dimensionless parameter measuring the distance from beam collapse (here we assume $\mathcal{P} \ll 1$) [32,36]. Expression (21) is recovered by setting $\delta = 0$ in

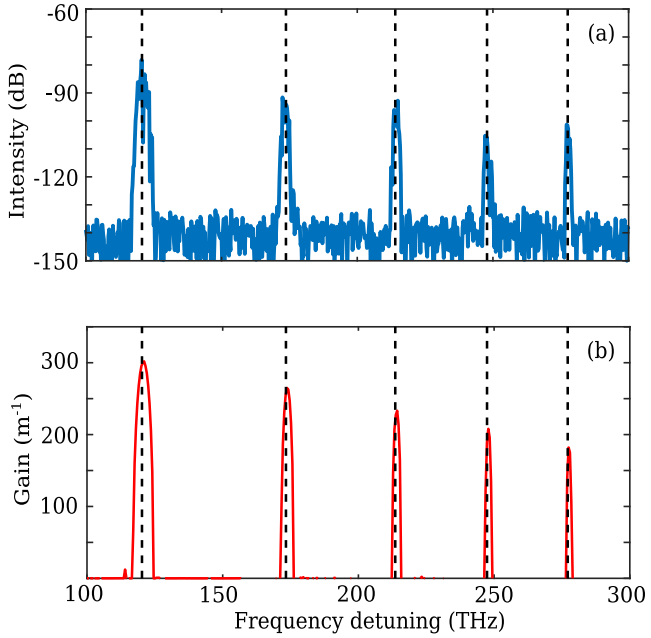


FIG. 4. The GPI gain for the uniform fiber case. (a) Output spectrum obtained by solving numerically the GNLSE (1). The black dashed lines correspond to unstable frequencies obtained from the parametric resonance condition (24). (b) Floquet spectrum obtained from Eq. (18). The parameters are $A_0^2 = 20$ GW/cm$^2$, $a_0 = 20$ $\mu$m, and fiber length 2.2 cm. The remaining parameters are as in Figs. 1(a) and 1(b).

Eqs. (5), (9), and (10). The average value of $F(z)$ can be calculated as

$$F_{av} = \frac{1}{\xi}\int_0^{\xi} F(z)dz = \frac{\chi A_0^2}{2\sqrt{\mathcal{C}}}. \tag{22}$$

The parametric resonance condition for Eq. (20), which reads

$$\frac{\beta_2\Omega^2}{2}\left(\frac{\beta_2\Omega^2}{2} + 2F_{av}\right) = \left(m\,\frac{\pi}{\xi}\right)^2, \tag{23}$$

permits us to find the central frequencies of the GPI bands as

$$\Omega_m^2 = \frac{2}{\beta_2}\left(-F_{av} + \sqrt{F_{av}^2 + g_0\,m^2}\right), \quad m = 1,2,\ldots. \tag{24}$$

The full GPI spectrum can be calculated by means of Floquet theory. This consists in solving the system (18) for two independent initial conditions (e.g., $[1,0]^T$ and $[0,1]^T$) over one period ($z = \xi$ in this case). This system can be solved only numerically because of the nontrivial form of $F(z)$. The two solutions calculated at $z = \xi$ compose the two columns of the $2 \times 2$ Floquet matrix, whose eigenvalues $\mu_1$ and $\mu_2$ determine the stability of the cw solution. If one eigenvalue (say, $\mu$) has modulus greater than one, the solution is unstable and the perturbations grow exponentially along $z$ with gain $G(\Omega) = \ln|\mu|/\xi$.

Figure 4 presents a comparison between the spectrum obtained from the numerical solution of the full GNLSE (1), starting from a cw perturbed by a small random noise, for a 2.2-cm-long uniform fiber [Fig. 4(a)] and the gain spectrum obtained from Floquet theory [Fig. 4(b)]. Vertical black dashed lines represent the frequencies $\Omega_m$ given by Eq. (24) for $m = 1,\ldots,5$, which are in excellent agreement with the locations of maximum gain. Note that in the low-intensity limit ($A_0 \to 0$), they can be approximated as $\Omega_m^2 \approx 2\pi m/\xi\beta_2$ [9]. The gain spectrum obtained from Floquet theory, plotted in Fig. 4(b), is in excellent agreement with the spectrum obtained from direct numerical simulation, plotted in Fig. 4(a), concerning the frequency and width of the gain bands, as well as their relative intensity.

### B. Varying core diameter

When the core diameter varies periodically, the spatial dynamics becomes richer and the self-imaging pattern is modulated, as described by Eqs. (5), (9), and (10) for $L_{\rm mod} \approx \xi$ or Eqs. (13) and (14) for $L_{\rm mod} \gg \xi$. As we will show in the following, this spatial dynamics generates additional GPI bands.

For the sake of simplicity, we consider a modulation period commensurate with the self-imaging distance, i.e., $p\,L_{\rm mod} = q\,\xi$ (where $p$ and $q$ are two integers). In this case the spatial evolution can be considered periodic with period $L = q\,\xi$, which allows us to obtain a simple analytic expression for the maxima of GPI gain. The parametric resonance condition for Eq. (20) reads now

$$\frac{\beta_2\Omega^2}{2}\left(\frac{\beta_2\Omega^2}{2} + 2F_{av}\right) = \left(m\,\frac{\pi}{L}\right)^2, \tag{25}$$

where we have assumed that the average nonlinear forcing term $F_{av}$ is the same as in the case of the uniform fiber. It is convenient to write the integer as $m = m_1 q + m_2$, which gives the following expression for the central frequencies of the GPI bands:

$$\Omega_{m_1,m_2}^2 = \frac{2}{\beta_2}\left[-F_{av} + \sqrt{F_{av}^2 + g_0\left(m_1 + \frac{m_2}{q}\right)^2}\right]. \tag{26}$$

The index $m_1 = 0,1,\ldots$ counts the main resonances, which correspond to the ones obtained in the uniform case for $m_2 = 0$ and $m_1 \neq 0$ [see Eq. (24)]. The most important information which can be extracted from Eq. (26) is that we have the generation of new sidebands around the principal ones. The number $m_2$ describes these additional subharmonic resonances deriving from the longer modulation period $L > \xi$. The interval of values for $m_2$ depends on the parity of $q$ and is defined formally for $q$ even as

$$q = 2n \Rightarrow \begin{cases} -n+1 \leqslant m_2 \leqslant n, & m_1 \neq 0 \\ 1 \leqslant m_2 \leqslant n, & m_1 = 0 \end{cases} \tag{27}$$

or odd as

$$q = 2n+1 \Rightarrow \begin{cases} -n \leqslant m_2 \leqslant n, & m_1 \neq 0 \\ 1 \leqslant m_2 \leqslant n, & m_1 = 0. \end{cases} \tag{28}$$

For example, we consider now a shallow modulation ($\delta = 0.12$) of the fiber, with a period $L_{\rm mod} = 8/7\xi$. Figure 5(a) reports the spectrum after a propagation of 3 cm from numerical simulations of the GNLSE (1). We can observe the characteristic splitting of bands due to the double periodicity. Black dashed lines show the frequency of unstable sidebands given by Eq. (24), which are in excellent agreement with the

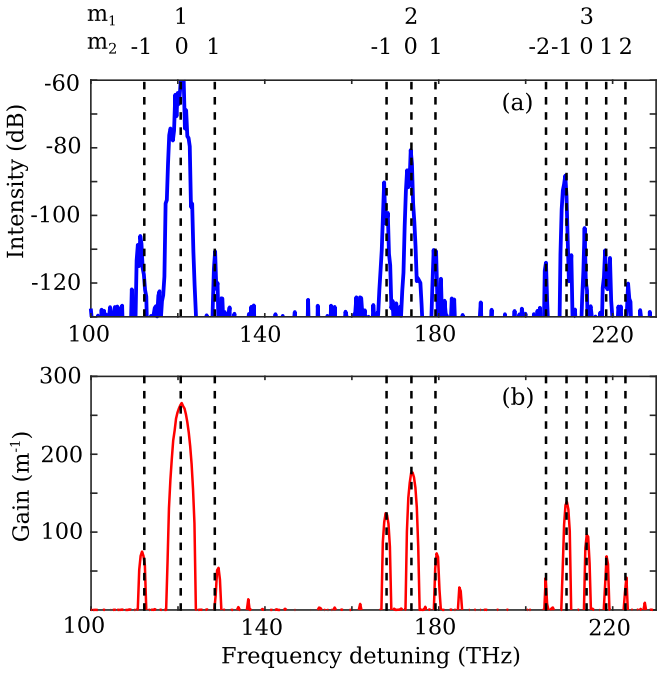


FIG. 5. Modulated fiber case. (a) Output spectrum obtained by solving numerically the GNLSE (1). The black dashed lines correspond to unstable frequencies obtained from Eq. (26). (b) Floquet spectrum obtained from Eq. (18). The parameters are $\delta = 0.12$, $L_{\mathrm{mod}} = (8/7)\xi$, $A_0^2 = 20$ GW/cm$^2$, and fiber length 3 cm. The remaining parameters are as in Figs. 1(a) and 1(b).

numerical simulation result. We can calculate the width and position of bands by performing a numerical Floquet analysis as described in the preceding section. As in the constant core case, the frequency, width, and relative intensity of the sidebands is in excellent agreement with numerical simulations [Fig. 5(a)].

It is interesting to investigate the gain spectrum as a function of the ratio $L_{\mathrm{mod}}/\xi$ between the modulation period and the self-imaging distance. We start by considering the range $L_{\mathrm{mod}} \approx \xi$, where the spatial moiré pattern is generated. Figure 6(a) shows the GPI gain map as a function of frequency and modulation period, calculated by means of the Floquet theory described before, using expressions (5), (9), and (10) for the beam size. The corresponding ratio between periods has been chosen to be commensurate and verifies $L_{\mathrm{mod}} = (n + 16)/(n + 12)\xi$, where $n$ is an integer in the interval $[0,20]$. The overall period of the spatial pattern is thus given by $L = (n + 16)\xi$. Remarkable agreement is found with the unstable frequencies predicted by Eq. (24), which are reported in Fig. 6(a) as black dashed curves. For each principal resonance $m_1 = 1,2,3$, one can notice the generation of additional sideband pairs $m_2 = \pm 4$, whose frequency separation increases with the modulation period. These additional sideband pairs appear at the index $m_2 = \pm 4$ because, for the definition of the modulation period used in this example, each value of $n$ generates an overall period $L$ composed of four slow oscillations (the pattern is quasiperiodic of period $\approx L/4$).

The other interesting case occurs when the modulation period of the core diameter is chosen to be several times greater than the self-imaging distance, i.e., $L_{\mathrm{mod}} \gg \xi$, where the spatial pattern is described by Eqs. (13) and (14). In this case, the relation between $L_{\mathrm{mod}}$ and $\xi$ has been chosen to verify $L_{\mathrm{mod}} = (12 + n)/4\xi$, where now $n$ is taken in the interval $[0,68]$, giving an overall period $L = (n + 12)\xi$. The corresponding Floquet gain map is reported in Fig. 6(b), where one can notice some qualitative differences. For the smallest modulation period, only a pair of sidebands appears, well detached from the fundamentals ones, corresponding to $m_1 = 1,2$. By increasing the modulation period, additional sideband pairs stem out and they all tend to cluster around the principal ones. For the longer modulation period considered here, at least three couples of sidebands merge with the fundamental ones, giving rise to a single structured band. Also in this case, remarkable agreement is found with the unstable frequencies predicted by Eq. (24) (black dashed curves).

The results of Floquet analysis are essentially supported by direct numerical integration of Eq. (1), as evidenced by Figs. 6(c) and 6(d), which report the output spectrum after a propagation distance of 3 cm as a function of $L_{\mathrm{mod}}$. In order to get rid of any randomness in the initial condition, we add a coherent seed to the cw (a short hyperbolic secant of duration 1 fs and intensity $10^{-5}$ smaller than the cw pump). Moreover, $L_{\mathrm{mod}}$ has been chosen to be equally spaced between the upper and lower limits considered, so the ratio of $L_{\mathrm{mod}}$ to $\xi$ is not necessarily commensurate. This fact confirms that considering the spatial behavior as strictly periodic does not produce any qualitative difference.

## V. CONCLUSION

We have studied theoretically GPI in a graded-index multimode fiber with an axially modulated core diameter. We have shown that a periodic modulation of the core diameter allows one to generate new GPI sidebands. We have developed a theory to predict the frequency of these additional sidebands, which is in excellent agreement with direct numerical simulations of the GNLSE and Floquet stability analysis. In our simulations we have used realistic parameters, which provides solid evidence that the described effects can be experimentally observed. Even if we assumed a circular symmetry of the problem throughout the paper, we verified by numerical simulations that the processes are robust with respect to perturbations such as fiber inhomogeneities or radially asymmetric input conditions. Our study contributes to a further understanding of the rich dynamics related to nonlinear waves propagating in multimode fibers. From an application point of view, the generation of multiple GPI sidebands in periodically modulated GRIN fibers can be exploited to optimize the spectral extent and/or the spectral power density of high-power supercontinuum sources based on highly multimode fibers.

## ACKNOWLEDGMENTS

The authors acknowledge discussions with G. Martinelli and O. Vanvincq. This work was partially supported by IRCICA; by the Agence Nationale de la Recherche through the NOAWE (Grant No. ANR-14-ACHN-0014) project, the LABEX CEMPI (Grant No. ANR-11-LABX-0007), and the

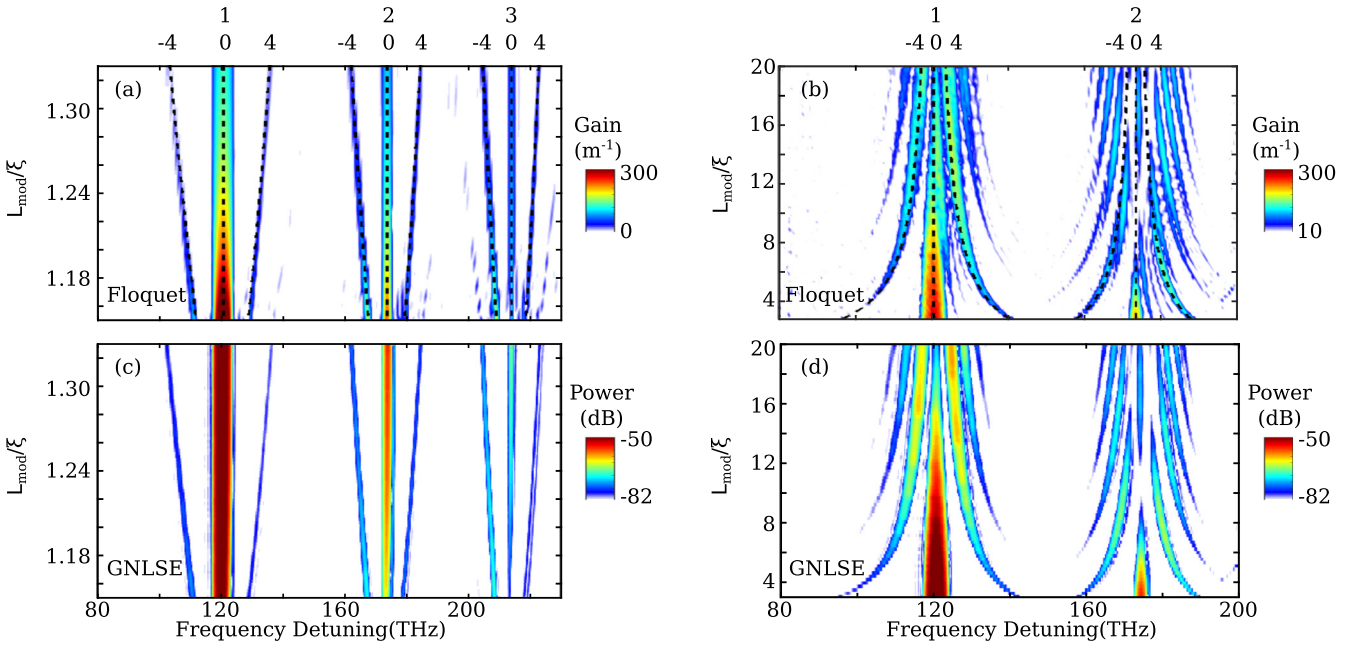


FIG. 6. (a) and (b) Gain map obtained with numerical Floquet analysis as a function of the ratio $L_{\mathrm{mod}}/\xi$ for (a) $L_{\mathrm{mod}} \approx \xi$ and (b) $L_{\mathrm{mod}} \gg \xi$. (c) and (d) Direct numerical integration of Eq. (2) for (c) $L_{\mathrm{mod}} \approx \xi$ and (d) $L_{\mathrm{mod}} \gg \xi$. The parameters are $\beta_2 = 16.55 \times 10^{-27}\ \mathrm{s}^2/\mathrm{m}$, $a_0 = 20\ \mu\mathrm{m}$, $\rho_0 = 26\ \mu\mathrm{m}$, and $A_0^2 = 20\,\mathrm{GW/cm}^2$.

Equipex Flux (Grant No. ANR-11-EQPX-0017 projects); by the Ministry of Higher Education and Research, Hauts-de-France Regional Council and European Regional Development Fund through the CPER Photonics for Society P4S.

## APPENDIX: MULTISCALE ANALYSIS

In this appendix, we give some details on the method used to approximate the beam evolution in the limit $L_{\mathrm{mod}} \approx \xi$. We start from Eq. (8), where we define the dimensionless coefficients $w = \sqrt{g}/k$, $\epsilon = w^2\delta$, and $\bar{z} = kz$ to get

$$\ddot{x} + \left(w^2 - 2\epsilon\cos(\bar{z}) + \frac{3\epsilon^2}{w^2}\cos^2(\bar{z})\right)x = 0. \tag{A1}$$

The initial assumption $L_{\mathrm{mod}} \approx \xi$ implies $w \approx 1$, thus we can safely perform a multiscale development in $\epsilon \ll 1$ [39] up to first order. By defining $\bar{z}_n = \epsilon^n \bar{z}$ and $x = \sum_{n=0} \epsilon^n x_n$ and equating equal powers of $\epsilon$, an infinite hierarchy of equations is obtained. From this infinite set equations, we retain only up to order $\epsilon^2$:

$$\left(D_0^2 + w^2\right)x_0 = 0 \quad \text{for } \epsilon^0, \tag{A2}$$

$$\left(D_0^2 + w^2\right)x_1 = -2[D_1 D_0 - \cos(\bar{z}_0)]x_0 \quad \text{for } \epsilon^1, \tag{A3}$$

$$\left(D_0^2 + w^2\right)x_2 = -2[D_1 D_0 - \cos(\bar{z}_0)]x_1 - \left(2D_2 D_0 + D_1^2 + \frac{3}{2w^3}\cos(\bar{z}_0)\right)x_0 \quad \text{for } \epsilon^2, \tag{A4}$$

where $D_n = \partial_{\bar{z}_n}$. At order $\epsilon^0$, we find

$$x_0 = A(\bar{z}_1, \bar{z}_2)e^{iwz} + A^*(\bar{z}_1, \bar{z}_2)e^{-iwz}, \tag{A5}$$

where $A(\bar{z}_1, \bar{z}_2)$ is a complex function depending on the slower variables $\bar{z}_1$ and $\bar{z}_2$. To know the dependence of this function on $z_1$ and $z_2$, Eq. (A5) is substituted in Eq. (A3) and secular terms are forced to vanish. We obtain the following solution for $x_1$:

$$x_1 = A(\bar{z}_2)\left(\frac{-e^{i(w+1)\bar{z}_0}}{2w+1} + \frac{e^{i(w-1)\bar{z}_0}}{2w-1}\right) + \text{c.c.}, \tag{A6}$$

where c.c. denotes the complex conjugate. To find $A(\bar{z}_2)$, we substitute $x_1$ in Eq. (A4) and impose again that secular terms vanish, resulting in

$$A = \frac{C}{2}e^{i(\phi\bar{z}_2 + \beta)}, \quad \phi = \frac{8w^2 - 3}{4w^3(4w^2 - 1)}, \tag{A7}$$

where $C$ and $\beta$ are two real constants fixed by the boundary conditions. By writing the complete function $x = x_0 + \epsilon x_1 + O(\epsilon^2)$, we obtain the general solution

$$x = C\left[\cos(\tilde{w}z+\beta) + \epsilon\left(\frac{\cos[(\tilde{w}-1)z+\beta]}{2w-1} - \frac{\cos[(\tilde{w}+1)z+\beta]}{2w+1}\right)\right] + O(\epsilon^2), \quad \tilde{w} = w\left(1+\frac{\delta^2(8\omega^2-3)}{4(4\omega^2-1)}\right). \tag{A8}$$

From this equation we can readily obtain $u(z)$ and $v(z)$ by imposing the appropriate boundary conditions.


[1] M. Faraday, On a peculiar class of acoustical figures; and on certain forms assumed by groups of particles upon vibrating elastic surfaces, Philos. Trans. R. Soc. London **121**, 299 (1831).

[2] M. C. Cross and P. C. Hohenberg, Pattern formation outside of equilibrium, Rev. Mod. Phys. **65**, 851 (1993).

[3] J. J. García-Ripoll, V. M. Pérez-García, and P. Torres, Extended Parametric Resonances in Nonlinear Schrödinger Systems, Phys. Rev. Lett. **83**, 1715 (1999).

[4] K. Staliunas, S. Longhi, and G. J. de Valcárcel, Faraday Patterns in Bose-Einstein Condensates, Phys. Rev. Lett. **89**, 210406 (2002).

[5] K. Staliunas, S. Longhi, and G. J. de Valcárcel, Faraday patterns in low-dimensional Bose-Einstein condensates, Phys. Rev. A **70**, 011601 (2004).

[6] P. Engels, C. Atherton, and M. A. Hoefer, Observation of Faraday Waves in a Bose-Einstein Condensate, Phys. Rev. Lett. **98**, 095301 (2007).

[7] S. J. Moon, M. D. Shattuck, C. Bizon, D. I. Goldman, J. B. Swift, and H. L. Swinney, Phase bubbles and spatiotemporal chaos in granular patterns, Phys. Rev. E **65**, 011301 (2001).

[8] V. Petrov, Q. Ouyang, and H. L. Swinney, Resonant pattern formation in a chemical system, Nature (London) **388**, 655 (1997).

[9] K. Krupa, A. Tonello, A. Barthélémy, V. Couderc, B. M. Shalaby, A. Bendahmane, G. Millot, and S. Wabnitz, Observation of Geometric Parametric Instability Induced by the Periodic Spatial Self-Imaging of Multimode Waves, Phys. Rev. Lett. **116**, 183901 (2016).

[10] Y. Kagan and L. A. Maksimov, Damping of trapped Bose-Einstein condensate oscillations at zero temperature, Phys. Rev. A **64**, 053610 (2001).

[11] G. Agrawal, *Nonlinear Fiber Optics* (Elsevier, Amsterdam, 2013).

[12] S. Pitois and G. Millot, Experimental observation of a new modulational instability spectral window induced by fourth-order dispersion in a normally dispersive single-mode optical fiber, Opt. Commun. **226**, 415 (2003).

[13] S. Wabnitz, Modulational polarization instability of light in a nonlinear birefringent dispersive medium, Phys. Rev. A **38**, 2018 (1988).

[14] M. Guasoni, Generalized modulational instability in multimode fibers: Wideband multimode parametric amplification, Phys. Rev. A **92**, 033849 (2015).

[15] R. Dupiol, A. Bendahmane, K. Krupa, J. Fatome, A. Tonello, M. Fabert, V. Couderc, S. Wabnitz, and G. Millot, Intermodal modulational instability in graded-index multimode optical fibers, Opt. Lett. **42**, 3419 (2017).

[16] F. Copie, M. Conforti, A. Kudlinski, A. Mussot, and S. Trillo, Competing Turing and Faraday Instabilities in Longitudinally Modulated Passive Resonators, Phys. Rev. Lett. **116**, 143901 (2016).

[17] M. Conforti, F. Copie, A. Mussot, A. Kudlinski, and S. Trillo, Parametric instabilities in modulated fiber ring cavities, Opt. Lett. **41**, 5027 (2016).

[18] F. Copie, M. Conforti, A. Kudlinski, A. Mussot, F. Biancalana, and S. Trillo, Instabilities in passive dispersion oscillating fiber ring cavities, Eur. Phys. J. D **71**, 133 (2017).

[19] A. Mussot, M. Conforti, S. Trillo, F. Copie, and A. Kudlinski, Modulation instability in dispersion oscillating fibers, Adv. Opt. Photon. **10**, 1 (2018).

[20] F. Matera, A. Mecozzi, M. Romagnoli, and M. Settembre, Sideband instability induced by periodic power variation in long-distance fiber links, Opt. Lett. **18**, 1499 (1993).

[21] A. Armaroli and F. Biancalana, Tunable modulational instability sidebands via parametric resonance in periodically tapered optical fibers, Opt. Express **20**, 25096 (2012).

[22] S. R. Nodari, M. Conforti, G. Dujardin, A. Kudlinski, A. Mussot, S. Trillo, and S. De Bièvre, Modulational instability in dispersion-kicked optical fibers, Phys. Rev. A **92**, 013810 (2015).

[23] C. Finot, J. Fatome, A. Sysoliatin, A. Kosolapov, and S. Wabnitz, Competing four-wave mixing processes in dispersion oscillating telecom fiber, Opt. Lett. **38**, 5361 (2013).

[24] M. Droques, A. Kudlinski, G. Bouwmans, G. Martinelli, and A. Mussot, Dynamics of the modulation instability spectrum in optical fibers with oscillating dispersion, Phys. Rev. A **87**, 013813 (2013).

[25] M. Droques, A. Kudlinski, G. Bouwmans, G. Martinelli, and A. Mussot, Experimental demonstration of modulation instability in an optical fiber with a periodic dispersion landscape, Opt. Lett. **37**, 4832 (2012).

[26] F. K. Abdullaev, S. A. Darmanyan, S. Bischoff, and M. P. Sørensen, Modulational instability of electromagnetic waves in media with varying nonlinearity, J. Opt. Soc. Am. B **14**, 27 (1997).

[27] K. Staliunas, C. Hang, and V. V. Konotop, Parametric patterns in optical fiber ring nonlinear resonators, Phys. Rev. A **88**, 023846 (2013).

[28] L. B. Soldano and E. C. M. Pennings, Optical multi-mode interference devices based on self-imaging: Principles and applications, J. Lightwave Technol. **13**, 615 (1995).

[29] A. Mafi, Pulse propagation in a short nonlinear graded-index multimode optical fiber, J. Lightwave Technol. **30**, 2803 (2012).

[30] L. G. Wright, S. Wabnitz, D. N. Christodoulides, and F. W. Wise, Ultrabroadband Dispersive Radiation by Spatiotemporal Oscillation of Multimode Waves, Phys. Rev. Lett. **115**, 223902 (2015).

[31] M. Conforti, C. M. Arabi, A. Mussot, and A. Kudlinski, Fast and accurate modeling of nonlinear pulse propagation in graded-index multimode fibers, Opt. Lett. **42**, 4004 (2017).

[32] S. Longhi, Modulational instability and space-time dynamics in nonlinear parabolic-index optical fibers, Opt. Lett. **28**, 2363 (2003).

[33] M. Guizar-Sicairos and J. C. Gutiérrez-Vega, Computation of quasi-discrete Hankel transforms of integer order for propagating optical wave fields, J. Opt. Soc. Am. A **21**, 53 (2004).

[34] F. Copie, A. Kudlinski, M. Conforti, G. Martinelli, and A. Mussot, Modulation instability in amplitude modulated dispersion oscillating fibers, Opt. Express **23**, 3869 (2015).

[35] V. M. Pérez-García, P. Torres, J. J. García-Ripoll, and H. Michinel, Moment analysis of paraxial propagation in a nonlinear graded index fibre, J. Opt. B **2**, 353 (2000).

[36] M. Karlsson, D. Anderson, M. Desaix, and M. Lisak, Dynamic effects of Kerr nonlinearity and spatial diffraction on self-phase modulation of optical pulses, Opt. Lett. **16**, 1373 (1991).

[37] E. Pinney, The nonlinear differential equation $y'' + p(x)y + cy^{-3} = 0$, Proc. Amer. Math. Soc. **1**, 681 (1950).

[38] J. F. Cariñena, A new approach to Ermakov systems and applications in quantum physics, Eur. Phys. J. Spec. Top. **160**, 51 (2008).

[39] A. H. Nayfeh and D. T. Mook, *Nonlinear Oscillations* (Wiley, New York, 1995).

[40] C. M. Bender and S. A. Orszag, *Advanced Mathematical Methods for Scientists and Engineers* (Springer, Berlin, 1999).